A Comprehensive Study of Module Layouts for Silicon Solar Cells Under Partial Shading

Nils Klasen, Florian Lux, Julian Weber, Torsten Roessler, and Achim Kraft

***Abstract*—Integrated applications for solar energy production becomes increasingly important. The electrification of car bodies and building facades are only two prominent examples. In such applications shading becomes a challenging problem, since the classic serial interconnection of solar cells in terms of power output is highly vulnerable to partial shading. In this article, we investigate the three most common module layouts in the market (conventional, butterfly, and shingle string) and add a fourth layout (shingle matrix) to be introduced to the market in the future. We discuss an approach to cluster shadings occurring in urban surroundings into basic shapes like "rectangular" and "random". Choosing a Monte Carlo technique in combination with latin hypercube sampling (LHS), we consider more than 3000 scenarios in total. For the evaluation of the scenarios, we conduct circuit simulations using LTspice. Furthermore, we define a normalization base, which considers only partial shading as a quantitative baseline for comparison. Our results show, that already for 200–400 scenarios the obtained output values stabilize. Among the investigated module layouts, the shingle matrix interconnection achieves the highest score, followed by a shingle string, half-cell butterfly and the conventional full-cell layout.**

***Index Terms*—LTspice simulations, partial shading, shading resilience, shingle matrix, shingling.**

I. Introduction

SHADING of a photovoltaic device stops its power generation, and even partial shading can amount to significant losses in the expected energy harvest. Investigations by Jahn and Nasse [1] show that for example in Germany 41% of the PV systems installed on roof tops are subjected to shading. This causes energy yield losses of up to 20% [1] and thus becomes especially relevant for the progressing electrification of various surfaces in urban environments like building facades or car bodies. Often, vegetation is a source of shading [3], [4], but also poles, chimneys and antennas have a contribution [5]–[7].

Manuscript received August 30, 2021; revised December 2, 2021; accepted January 15, 2022. Date of publication February 8, 2022; date of current version February 19, 2022. This work was supported in part by the German Federal Ministry of Economic Affairs and Energy (BMWi) under Grant 03EE1026A, acronym Shirkan, and in part by German Environmental Foundation (DBU) under graduate scholarship program. *(Corresponding author: Nils Klasen.)*

Nils Klasen is with the Fraunhofer Institute for Solar Energy Systems ISE, 79110 Freiburg, Germany, and also with the Karlsruhe Institute of Technology, Institute for Applied Materials—Material and Biomechanics IAM-WBM, 76344 Eggenstein-Leopoldshafen, Germany (e-mail: nils.klasen@ise.fraunhofer.de).

Florian Lux, Julian Weber, Torsten Roessler, and Achim Kraft are with the Fraunhofer Institute for Solar Energy Systems ISE, 79110 Freiburg, Germany (e-mail: florian.lux@ise.fraunhofer.de; julian.weber@ise.fraunhofer.de; torsten.roessler@ise.fraunhofer.de; achim.kraft@ise.fraunhofer.de).

Color versions of one or more figures in this article are available at https://doi.org/10.1109/JPHOTOV.2022.3144635.

Digital Object Identifier 10.1109/JPHOTOV.2022.3144635

Within the recent years, there has been a diversification of PV module products and new module layouts like a "butterfly" for half-cut solar cells, shingle strings [8] or matrix shingling [9] have been introduced as alternatives to the "conventional" strict series interconnection of full wafer cells. Within the latter, the most common measure to reduce power generation losses caused by shading, is the implementation of bypass diodes in parallel to the solar cell strings [10], [11]. By reducing the reverse bias on shaded solar cells, bypassing also mitigates the risk of hotspot formation on shaded solar cells.

Investigations of solar module layouts show some similarities to studies investigating solar array topologies [12] where *e.g.*, the "total-cross-tied" configuration basically is a scaled to power plant version of the shingle matrix approach [13]. Often, the strategy to encounter the problem of mismatching currents when shading occurs is to implement parallel interconnections [14] or increase the number of bypass diodes per module [15]. Studies of partial shading in urban surroundings often consider specific shading conditions to gain an energy yield predictions [14] for different configurations of both module and array interconnection scheme. In this article, we want to investigate today's most common module topology with the aim to rate their suitability for the application in an urban environment.

Half-cut solar cells and 1/5th or 1/6th shingle solar cells offer a new flexibility to combine serial and parallel interconnections of solar cells and thereby enhance the power output under partial shading [6]. According to the ITRPV, the conventional strict serial interconnection of solar cells will soon be replaced [16]. To account for the different shading responses of these new module layouts, we conducted a comprehensive study over a large set of shading scenarios. By considering the irradiation inhomogeneity between shaded and unshaded parts in a normalization factor, we can compare the module layouts regarding their partial shading response. Circuit simulations based on SPICE are widely used to compute *I–V* characteristics of solar power generators and to yield precise predictions of their power outputs in different irradiation scenarios [17]–[19].

A key feature of our work are Monte Carlo shading scenarios to form representative sets for two basic shading shapes (rectangular and random). With these, we aim to cover a significant fraction of shadings occurring in an urban environment. The scenarios are created so that they span the entire range from unshaded to fully shaded cases in many small steps and different shapes. This is a significant extension over investigating only a small number of specific shading scenarios, such as a gradual

shading along the module edges or shading of single solar cells within a solar module [20]–[23].

II. Methodology

A. Evaluation of the Shading Scenarios

So far, few studies have been dedicated to defining a quantity describing the shading tolerability of photovoltaic. Often, circuit simulations based on a one or two diode representation for the *I–V* characteristic of the solar cells are used to evaluate and compare different interconnection approaches with respect to their power output in specific shading scenarios [23], [24]. Typically only few and simple scenarios are investigated [25]. However, a universal evaluation of the performance of a solar module under partial shading requires a statistical approach aiming to cover at least a substantial fraction of the numerous shading scenarios occurring in field operation.

The first who worked toward the definition of a universal quantity ST to compare the shading response of PV generators were Ziar *et al.* [2]. In their work, they derive an expression for the permutation of all possible configurations of i irradiation levels between 0 and 1 kW m^{-2} on n solar cells in a serial interconnection and m parallel interconnected strings; j is defined as $j = i - 1$ (for more details on the expression and its derivation please refer to [2])

$$\mathrm{ST}_{c,i} = \frac{m}{nm}\frac{1}{i^n} \times \left[\sum_{k=1}^{j}\binom{n}{j}k + \sum_{a=1}^{j-1} n\binom{j-a}{j}\sum_{b=1}^{n-1}\binom{n}{b}a^{n-b}\right]. \quad (1)$$

The permutation considers uniform shading across the full solar cells. According to findings by Quaschning *et al.* [26] this is a valid assumption. Moreover, their results imply that uniform irradiation level on cell level also considers all inhomogeneous cases, thus varying shading shapes on cell level, within a small error of $\sim$2% at the MPP. In the following we refer to this as the *irradiation equality*. This principle is also used by Meyer *et al.* when investigating shading in PV arrays by a neural network machine learning algorithm [27].

Ziar *et al.* [2] show, that their permutation formula for $i \to \infty$ irradiation levels approaches the following equation which makes n the only relevant factor influencing ST

$$\lim_{i\to\infty} : \mathrm{ST} = \frac{1}{n+1}\,. \quad (2)$$

Our interpretation of (1) $|_{i\to\infty} =$ (2) is a lower physical boundary for what a solar module can yield when subjected to partial shading. However, in commercial solar modules several measures can be taken to reduce the vulnerability against partial shading like bypass diodes, but also using half-cut or shingle solar cells, which then produce currents spatially distributed in parallel interconnections and therefore are less likely to be shaded at the same time. Ziar *et al.* [2] add a factor λ to account for such measures

$$\mathrm{ST} = \lambda\frac{1}{n+1}. \quad (3)$$

An analytical description for λ is not found yet and ST therefore can only be accessed by experiments [2]. This requires the investigation of different shading scenarios, evaluation of the resulting module power for each case followed by an averaging and normalization procedure. Mishra *et al.* [28] are working on splitting λ into different contributions and so far managed to resolve temperature effects during operation. However, the important contributions of bypass diodes or the spatial distribution and interconnection scheme of the solar cells of different sizes to λ are still not found.

Other work by Wang and Sheu [29] tries to find analytical descriptions of probability densities for random shading of solar cells. However, they also fail to find analytical representations for the effect of bypass diodes and continue with numerical values obtained by Monte Carlo simulations.

In conclusion, it appears that analytical representations of (partial) shading of solar modules is very hard if not impossible to achieve. Therefore, we pursuit a Monte Carlo approach to find reliable average power values. The Monte Carlo technique is considered very powerful when probabilities are hard to describe in an analytically closed form. We choose simulations which offer major advantages in terms of speed and reproducibility when it comes to the evaluation of many complex scenarios. SPICE simulations are known to predict solar cell characteristics with a high precision and are therefore also used to, e.g., verify simplified electrical models of solar power generators [27]. Therefore, we chose the state-of-the-art SPICE approach using the open-source code LTspice. The representation of solar cell characteristics are discussed in Section II-B, the chosen approaches to model shading in Section II-D. In our simulations we consider STC conditions excluding effects like temperature changes in field operation. A validation of the electrical model has been published previously and underlines its reliability [30].

In the following paragraph we discuss the averaging and normalization procedure of this article. Shading scenarios are randomly created and follow the constraint of an equidistant distribution regarding their shaded area fraction $A_{\mathrm{sh}} = A/A_0$ with the shaded area A and the module area A_0. This is shown exemplarily for the power data points $P(A_{\mathrm{sh}})$ in Fig. 1. For equidistant steps of the differential on a scale from 0 to 1 the integration of $P(A_{\mathrm{sh}})$ yields an average value of P. It is an important condition in our approach that the shading scenarios cover the entire range from unshaded to fully shaded without the formation of "clusters" of data points by means of identical shaded area fractions in multiple scenarios. This demand aims to consider the entire spectrum equally in the obtained average power value while at the same time still considering many possible scenarios.

Fig. 1 also shows two limit functions $P_{\min}$ and $P_{\max}$. $P_{\max}$ represents the upper physical limit for the power output under the assumption of independent operating solar cells following the *irradiation equality*. $P_{\min}$ represents the lowest possible power output, i.e., when the solar module is shaded completely

$$P_{\max} = P_0\ (1 - (1 - I_{\mathrm{SO}}) \cdot A_{sh}) \quad (4)$$

$$P_{\min} = I_{\mathrm{SO}}\ \cdot P_0. \quad (5)$$

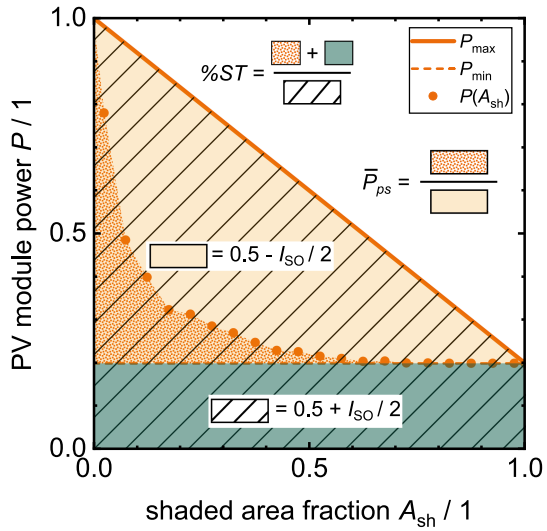

Fig. 1. Graphical comparison of the relative Shading Tolerability %ST [2] and the average normalized power for partial shading $\bar{P}_{\mathrm{ps}}$. The case depicted here corresponds to an irradiation on shaded areas of $I_{\mathrm{SO}} = 0.2$ kW m^{-2}. The data points show an exemplary function of the module power $P(A_{\mathrm{sh}})$ computed by LTspice circuit simulations. The solid line shows the ideal, upper limit P_{max} for independent operating solar cells while the dashed line shows the lower limit P_{min} corresponding to a fully shaded solar module.

In (4) and (5) P_0 is the power output without shading, i.e., $A_{\mathrm{sh}} = 0$. I_{SO} represents the fraction I/I_0 of the global irradiation I_0 reaching the solar cells behind the shading object due to scattering (sky, surrounding objects), reflection (surrounding objects) or transmission (semitransparent objects [31]). To maintain one terminology we adopt this notation from Ziar *et al.* [2].

We propose to consider only the inhomogeneous fraction of the irradiation for the evaluation. We motivate this by the fact that differences in the response of solar modules to partial shading originate from the current mismatch, i.e., the irradiation mismatch between shaded and unshaded parts. Therefore, we exclude the baseline irradiation I_{SO} by subtraction from the evaluation. This results in the evaluation of the average normalized power for partial shading $\bar{P}_{\mathrm{ps}}$ given as

$$\bar{P}_{\mathrm{ps}} = \frac{\int_0^1 P\left(A_{\mathrm{sh}}\right) - P_{\mathrm{min}}\,\mathrm{d}A_{\mathrm{sh}}}{\int_0^1 P_{\mathrm{max}} - P_{\mathrm{min}}\;\mathrm{d}A_{\mathrm{sh}}}\,. \tag{6}$$

Its graphical representation is given in Fig. 1 by the fraction of the highlighted areas as well as a graphical representation of the experimental evaluation according to Ziar *et al.* [2]. The difference between both is given by the green rectangle below P_{min}. In [2], the normalization is represented by the striped area below P_{max} which evaluates to $0.5 + I_{\mathrm{SO}}/2$ considering $A_{\mathrm{sh}} = 0$ to 1. In this article, it is equal to $0.5 - I_{\mathrm{SO}}/2$. Combining (4)–(6) and partially solving the integration for A_{sh} in the boundaries from 0 to 1, $\bar{P}_{\mathrm{ps}}$ is given by (7). The integration of $P(A_{\mathrm{sh}})$ is done numerically using the trapezoidal rule

$$\bar{P}_{\mathrm{ps}} = \frac{2}{\left(1 - I_{\mathrm{SO}}\right) P_0} \int_0^1 P\left(A_{\mathrm{sh}}\right) \mathrm{d}A_{\mathrm{sh}} - \frac{2 I_{\mathrm{SO}}}{1 - I_{\mathrm{SO}}}. \tag{7}$$

Since this approach relies on the Monte Carlo principle, $P(A_{\mathrm{sh}})$ requires an adequate number of data points to obtain robust values for $\bar{P}_{\mathrm{ps}}$. Therefore, this method also depends on the strategy to create sets of representative shading scenarios for the evaluation of $\bar{P}_{\mathrm{ps}}$. This is further discussed in Sections II-D and III-A.

B. Solar Cell Characteristics

There are only minor variations in today's industrial solar cell manufacturing within each power bin. However, we also cover these slight differences in our simulations. Therefore, we characterize a set of 30 solar cells. In the simulation setup the different characteristics are described by the extended two-diode model and distributed randomly across the simulated PV module circuit. The extension of the two-diode model includes the entire characteristic under reverse bias until break down. The reverse break down characteristic is represented by a Schottky-diode term as proposed by Rauschenbach [32]

$$\begin{aligned} J\ (V) = J_{\mathrm{ph}} &- J_0 \left(\exp\left\{ \frac{e\left(V + JR_{\mathrm{s}}\right)}{k_{\mathrm{B}} T n_0} \right\} - 1 \right) \\ &- J_1 \left(\exp\left\{ \frac{e\left(V + JR_{\mathrm{s}}\right)}{k_{\mathrm{B}} T n_1} \right\} - 1 \right) \\ &+ J_{\mathrm{Br}} \exp\left\{ -\frac{e\left(V + JR_{\mathrm{s}} - V_{\mathrm{Br}}\right)}{k_{\mathrm{B}} T n_{\mathrm{Br}}} \right\} - \frac{V + JR_{\mathrm{s}}}{R_{\mathrm{p}}}. \end{aligned} \tag{8}$$

Compared to the most commonly used Bishop model [33], the Rauschenbach [32] approach is less complex to implement. Only three additional parameters are needed in LTspice: The reverse breakdown voltage V_{Br}, the breakdown avalanche factor n_{Br} and the diode saturation current density J_{Br}. We treat the n_{Br} as a fit parameter including the ideality factor of the reverse break down diode. In LTspice the reverse breakdown parameters are added to the second diode D_1. In summary, the current-voltage characteristic of the solar cells is represented in(8). The ideality factors are set to $n_0 = 1$ and $n_1 = 2$.

Fig. 2 shows an exemplary *I–V* curve of one of the characterized commercial passivated emmiter and rear contact (PERC) shingle solar cells. We find good agreement between the measured data and both the numerical solution of (8) (solid line) and an LTspice simulation (dashed line) with the corresponding set of parameters. Recent findings by Clement *et al.* [34] show, that for some cell architecture, the reverse bias characteristic can be significantly influenced by the irradiation level. We do not consider this in the article, but find it important to point it out.

The solar cells are characterized under standard test conditions (1 kW m^{-2}, $AM1.5$, 25 °C) in a *Halm Cetis Celltest3* cell tester under forward bias. Since the reverse breakdown voltage is out of the operating range of the cell tester, the reverse data is obtained in a laboratory setup under zero illumination. After combining both data sets, (8) is fitted to the data by the least square method. Furthermore, the *I–V* characteristic is simulated by means of LTspice.

As simulation input, we take the two-diode parameters obtained for shingle solar cells and scale them to half-cut and full-sized solar cells.

TABLE I
EXTENDED TWO DIODE PARAMETERS OBTAINED BY FITTING (8) TO THE MEASUREMENT DATA. EACH GROUP CONTAINS 30 SOLAR CELLS

	J_{ph} / mA cm^{-2}	J_0 / pA cm^{-2}	J_1 / nA cm^{-2}	V_{Br} / V	n_{Br} / 1	J_{Br} / A cm^{-2}	R_s / Ω cm^2	R_p / kΩ cm^2
Commercial	39.64	0.11	23.7	−29.7	27.8	570	0.56	130
PERC	±0.00	±0.01	±5.5	±1.5	±5.2	±140	± 0.07	±130

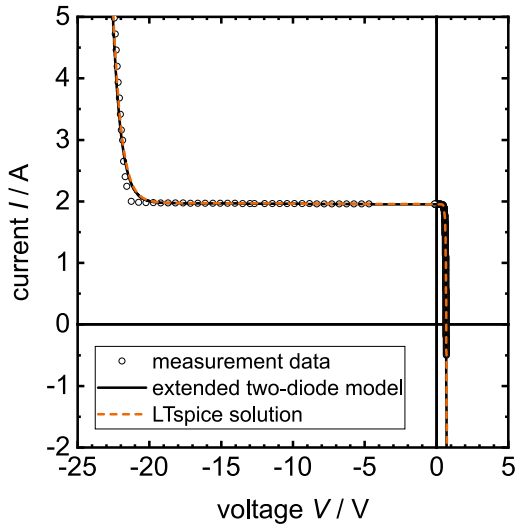

Fig. 2. Exemplary *I–V* characteristic of an industrial PERC shingle solar cell measured for setting up the LTspice module simulations. The data points show measurement data, the solid line the numerical approximation of (8) and the dashed line the result of an LTspice simulation with the corresponding set of parameters.

Table I gives the parameters of the extended two diode model for 30 commercial PERC shingle solar cells. The data refer to the characteristics after separation. Errors represent standard deviation found within the group. For more details on characterization, modeling and validation of this approach, please refer to our previous work [13].

C. Module Layouts

We compare four different module layouts based on three different solar cell sizes: M2 full-sized; M2 half-cut; and M2 1/5th shingle solar cells. The module layouts are shown in Fig. 3: a) the conventional interconnection of full-sized solar cells; b) the so-called butterfly layout for half-cut solar cells; c) the shingle string layout; and d) the shingle matrix layout. For better comparability each module consists of the same number of full-cell equivalents, although the shingle interconnection in principle allows the integration of a higher number of full-cell equivalents on the same module surface due to the overlap of the solar cells.

Layouts a) to c) represent the majority of today's commercially available layouts for crystalline silicon solar modules which currently are estimated to cover 95% of the world market for photovoltaics [16]. Additionally, the shingle matrix layout [30] is investigated as a promising candidate to further improve the shading resilience of solar module products. We do not consider "dynamic" module layouts which use, e.g., submodule switches to rearrange the interconnection-scheme within the solar module [35], since they are still subject to research and have not yet been introduced to the market. However, they could be investigated using this method by implementing their static configurations and then for each scenario pick the configuration with the highest output. This assumes that the "dynamic" part of the solar module is capable of always finding the optimal configuration and is not limited by external conditions like, e.g., a maximum output current.

The described method is applicable on any solar module layout and is also comparable for different solar module sizes. Challenges involve proper characterization and modeling of the entire *I–V* curve of the solar cells, since often *I–V* testers cannot access high enough negative voltages to include the reverse breakdown regime. For solar modules of different sizes, shading scenarios should be scaled accordingly.

While the assignment of solar cells in the considered PV modules is shown in the upper part of Fig. 3, the electrical interconnection is sketched in the lower part, including the implementation of three bypass diodes. The butterfly layout consists of two parallel interconnected blocks of solar cells, which are divided by the bypass diodes arranged in the center. The shingle string interconnection consists of six parallel interconnected strings, which are intermitted by the three bypass diodes, resulting in three serial interconnected blocks of solar cells. In the shingle matrix interconnection, each individual solar cell is interconnected in series and parallel to its neighbors. This is best described as a serial interconnection of rows of parallel interconnected solar cells. Hence, each row can be considered to perform like a single (long) solar cell. In this sense, the matrix interconnection is like typical thin film solar modules consisting of long, rectangular-shaped solar cells.

Note that the solar cells are interconnected by electrical resistors R_{lat} modelling a lateral current transport as discussed in [13]. However, R_{lat} only becomes relevant in the matrix shingle layout when partial shading forces currents to flow along the parallel interconnection of the solar cells to bypass shaded areas. Values for R_{lat} range from 100 to 400 $\mathrm{m}\Omega$ [13]. For comparability also full sized solar cells and half-cut solar cells are equipped with these lateral resistors on sub-cell level. Thus, they have no effect in these layouts. The series resistance of the interconnection was assumed to be 10 $\mathrm{m}\Omega$ for all layouts and has been added to the R_{s} in the two diode model.

D. Shading Scenarios

Since we use identical numbers of full cell equivalents all shading scenarios are directly transferrable. For simplicity, we neglect minor geometrical differences like cell and string gaps in real PV modules and virtually place all solar cells without any gaps, to eliminate such distracting differences. We set the irradiation on shaded areas to zero $I_{\mathrm{SO}} = 0$.

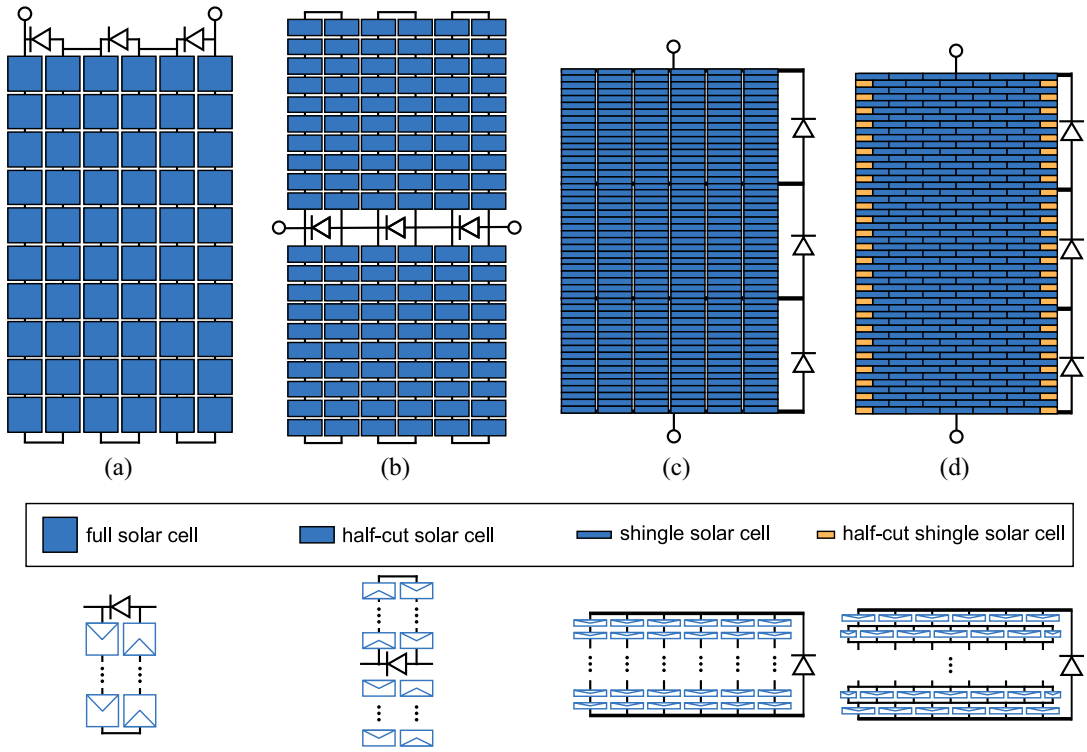

Fig. 3. Module layouts investigated in this article a conventional full-sized solar cell interconnection b half-cut solar cell butterfly layout with centered diodes and two parallel blocks of solar cells above and below c shingle string interconnection with six parallel strings of shingle solar cells intermitted by three diodes d shingle matrix interconnection with serial and parallel interconnection of each individual solar cell. Note that in case of the shingle matrix layout, half-cut shingle solar cells are introduced to form a rectangular module shape. Furthermore, not sketched, the solar cells are interconnected by a lateral resistance as discussed in [10].

To find meaningful values for $\bar{P}_{\mathrm{ps}}$, we define two basic shapes of shadings. With these we aim to cover a significant fraction of shadings occurring in an urban environment. Often other solar modules, buildings, parts of building (chimneys, antennae, or poles) cause rectangular shades either in the center of a module or starting from the edge reaching into the center. We consider such cases by defining a rectangular shading shape. Other often observed shadings originate from leaves, bird droppings, and vegetation in any form. We consider these cases by randomly shaped shadings.

Rectangular scenarios are defined by their position $\vec{C}_{\mathrm{sh}} = (x\ y)^{\mathrm{T}}$ on the module surface, their rotation angle α_{sh} towards the x-axis and their width w_{sh}. Orthogonal to w_{sh} the shadow expands infinitely in these simulations. The shaded area fraction is computed from these four parameters for each scenario.

Random shading scenarios are built from pixels which can either be illuminated or shaded. Its governing parameters are the shaded area fraction A_{sh} and the maximum number of shadings n_{sh}. Since shingle solar cells represent the smallest unit, we create the scenarios for these layouts and transfer them to the other layouts by, e.g., summarizing five shingle solar cells to form the spatially corresponding full sized solar cell. Each shingle solar cell is split into 25×25 pixels. Starting from random seed pixels on the module surface, neighboring pixels are randomly chosen one-by-one to be shaded. Again, following the *irradiation equality*, we evaluate the average irradiation of all pixels assigned to a solar cell. The number of pixels to be shaded is directly defined by the shaded area fraction of each scenario. n_{sh} defines the maximum number of shadings, *i.e.*, for each scenario the total A_{sh} is distributed randomly on a randomly chosen number of shadings from 1 to n_{sh}. Shadings are allowed to touch and merge but not to overlap.

Fig. 4 shows examples for the two basic shading cases. First, shaded module areas are computed followed by the assignment of the total irradiation on the individual solar cells. Following the *irradiation equality*, the photocurrent of each solar cell is computed and forwarded to LTspice as input for the circuit model. More details on the performed simulations are given in Section III.

E. Governing of the Parameters Defining the Shadings

Since high values for n_{sh} tend to behave like a spatial homogeneous reduction of the irradiation (imaging distributing A_{sh} on 500 pieces of shading on the module surface), n_{sh} is set to a constant value and not varied within the studies. This leaves A_{sh} as the only independent variable and we can simply vary A_{sh} for any number of scenarios.

In case of rectangular shading, we have four independent variables creating a large space of possible combinations. We, therefore, use latin hypercube sampling (LHS) [36] to define parameter combinations. Following the conclusion of Helton and Davis [36] on different sampling strategies, "Monte Carlo analysis with LHS is the most broadly applicable approach to

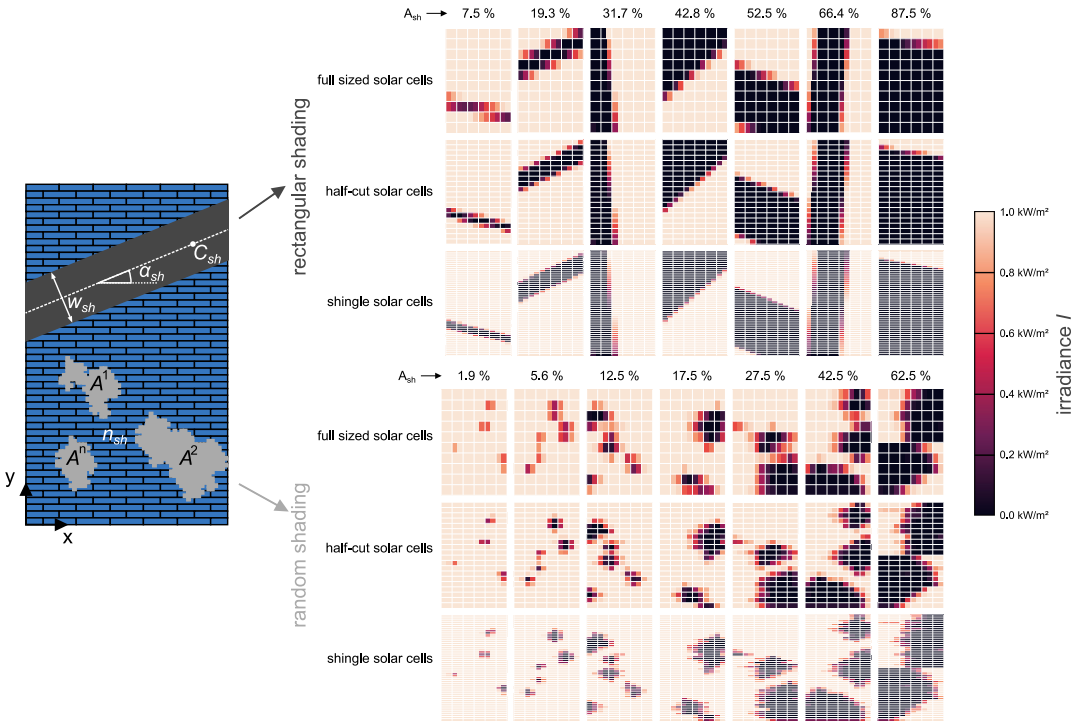

Fig. 4. Shading scenarios investigated in the simulations. Seven exemplary shading scenarios given by their irradiation map are shown for both basic shading cases and all three solar cell formats. Rectangular shadows are defined by their x- and y-position $C_{\mathrm{sh}} = (x|y)$ on the module surface, their angle α_{sh} toward the x-axis and the width w_{sh}. The length of the shadow expands infinitely. Random shading is defined by the number of shadows $n_{\mathrm{sh}} = 10$ and varying A_{sh} , which is defined by $A_{\mathrm{sh}} = \sum A^{\mathrm{n}}$.

the propagation and analysis of uncertainty and often the only approach needed" [36]. As described by McKay *et al.* [37] LHS combines and extends random quota sampling [38] and latin square sampling [39]. The latter goes back to Euler, who by using latin letters named this technique of distributing two parameters. The extension to an n-dimensional parameter space subsequently is called LHS. Each parameter range is divided into x equidistant steps. Now k n-tupel are formed so that there are no similar values in any parameter or expressed differently: Every step value of a parameter is used exactly once. This reduces the x^n possible parameter combinations to x combinations while at the same time distributing the parameter values evenly in the n-dimensional space.

TABLE II
PARAMETER LIMITS FOR LHS OF THE RECTANGULAR SHADING SCENARIOS

Parameter	Lower limit	Upper limit
x / mm	0	$l_{\mathrm{M}} = 1567.5$
y / mm	0	$w_{\mathrm{M}} = 940.5$
α_{sh} / °	0	90
w_{sh} / mm	0	$2\sqrt{l_{\mathrm{m}}^2 + w_{\mathrm{M}}^2} = 3656.0$

F

III. SIMULATIONS

A. Robustness of $\bar{P}_{ps}$

Prior to the determinations for the module layouts, we investigate the robustness of $\bar{P}_{ps}$. We created sets of random shading patterns ranging from 10 to 1250 scenarios per data point. $\bar{P}_{ps}$ is determined for all module layouts.

For the rectangular shadings, we use subsets of the entire data set for the robustness evaluation. Data points are sorted by A_{sh} and then split into sets of equidistant data points. For evaluation of $\bar{P}_{ps}$ we then randomly choose one of the datasets.

B. Determination of $\bar{P}_{ps}$ for Relevant Module Layouts

In our simulations we set I_{SO} equal to 0 kW m^{-2}. Table II gives the boundary values for the four parameters defining the rectangular shading case. The boundaries are defined so that a total coverage of the solar module is possible for any combination of x, y, α_{sh}, and w_{sh}. Since w_{sh} expands symmetrically around C_{sh} its upper boundary value must be set to twice the module diagonal to consider the case $x = y = 0$ mm and $A_{\mathrm{sh}} \overset{!}{=} 1$. Note, that we consider a full cell equivalent with the size of 156.75 × 156.75 mm. We set the number of parameter combinations to be created by LHS to 2000. The resulting A_{sh} for each scenario is computed from the set of parameters.

Examining the set of scenarios, we find, that due to the boundaries set for the LHS, there are 777 scenarios with a shaded area fraction of $A_{\mathrm{sh}} = 1$. This results from the demand, that $A_{\mathrm{sh}} = 1$ should be a possible outcome for each parameter set. This still leaves 1223 scenarios with values of A_{sh} from 0 to 1.

Subsequently, we set the number of random scenarios to approximately the same value (1250 scenarios). We set $n_{\mathrm{sh}} = 10$ and distribute A_{sh} equidistantly into 1250 steps from 0 to 1.

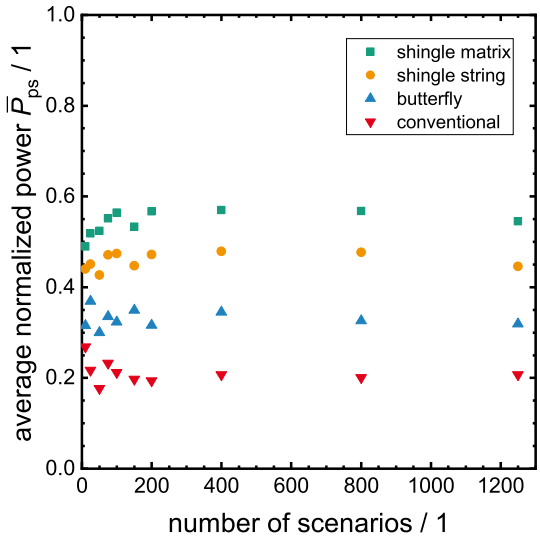

Fig. 5. Values of $\bar{P}_{\mathrm{ps}}$ obtained for varying numbers of rectangular scenarios evaluated according to (7). The values for $\bar{P}_{\mathrm{ps}}$ appear to converge for more than 200 considered scenarios. The data points are evaluated from random subsets of the entire data set.

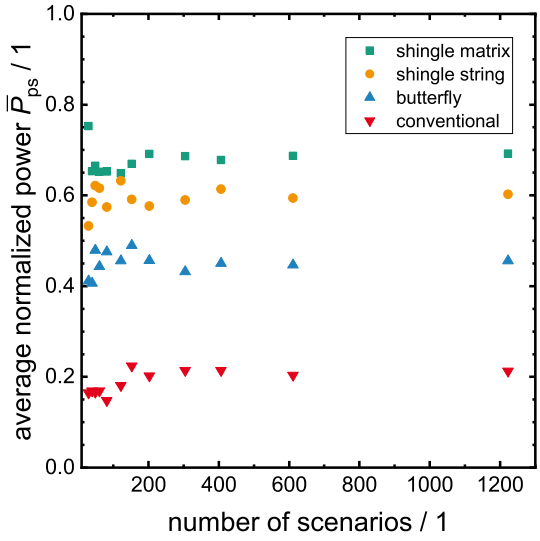

Fig. 6. Values of $\bar{\boldsymbol{P}}_{\mathbf{ps}}$ obtained for varying numbers of random shading scenarios. For each step a new set of scenarios was created.

IV. Results and Discussion

A. Robustness of $\bar{\boldsymbol{P}}_{\boldsymbol{ps}}$

In Fig. 5 is plotted against the number of rectangular shading scenarios for the evaluation of $\bar{P}_{ps}$. For values larger than 200 we find $\bar{P}_{\mathrm{ps}} = 0.687 \pm 0.005$ for the shingle matrix layout, $\bar{P}_{\mathrm{ps}} = 0.595 \pm 0.013$ for the shingle string layout, $\bar{P}_{\mathrm{ps}} = 0.448 \pm 0.008$ for the butterfly layout and $\bar{P}_{\mathrm{ps}} = 0.209 \pm 0.005$ for the conventional layout. The errors refer to the standard deviation on the considered data points. From the course of the plotted data and the low errors we conclude, that for a number larger than 200 scenarios $\bar{P}_{\mathrm{ps}}$ is a robust value.

Fig. 6 shows $\bar{P}_{\mathrm{ps}}$ a similar evaluation for the random scenarios. Again $\bar{P}_{\mathrm{ps}}$ is plotted against the number of scenarios. For values larger than 200 we find $\bar{P}_{\mathrm{ps}} = 0.563 \pm 0.010$ for the matrix layout, $\bar{P}_{\mathrm{ps}} = 0.469 \pm 0.013$ for the string layout, $\bar{P}_{\mathrm{ps}} = 0.327 \pm 0.011$ for the butterfly layout and $\bar{P}_{\mathrm{ps}} = 0.202 \pm 0.005$ for the conventional layout. Again, we find that $\bar{P}_{ps}$ shows robust values for a relatively small number of scenarios (compared to the consideration of infinite scenarios).

In both cases the values found for 200 as well as the maximum number of scenarios are already within the projected final range. We conclude that this method is applicable to investigate the partial shading response of arbitrary module layouts subjected to clusters of random shading. With cluster we address the definition of a basic shading shape like rectangular or random and the generation of a set of random shadings similar to the basic scenario.

It is obvious from these findings that the absolute value for $\bar{P}_{\mathrm{ps}}$ is a function of the chosen basic shading case. However, this is the first step towards a case-sensitive quantification of the response to partial shading. Next steps would be the definition of further basic cases if needed, e.g., branch-like random structures (rather than random spherical ones). A set of $\bar{P}_{\mathrm{ps}}$-values for different basic shading scenarios could then define a shading response vector which could be multiplied by a weighting-vector for different locations, such as roof-tops (almost only rectangular shapes), facades (mixture of random and rectangular), vehicle integration (mixture of random and rectangular). Such a strategy is a possible solution to gain reliable information on the response of future solar module layouts to partial shading.

Although 200 scenarios appear to be sufficient, a larger number of scenarios offers further insight, e.g., into effects originating from conductive bypass diode states.

B. $\bar{\boldsymbol{P}}_{\mathbf{ps}}$ for Rectangular Shading

Fig. 7 shows the results for rectangular shading scenarios and the four module layouts as indicated in the legend of each layer. Each data point corresponds to one scenario. The area below the data is highlighted for each set. Note, that for some data points the area below is too thin to be displayed with the given resolution of the x-axis. From the obtained distribution of the data, it is obvious that the relationship between shaded area fraction and PV module power can hardly be described by reasonable mathematical function. However, with the integration of the complete dataset, we provide suitable basis for comparison between different layouts.

Besides the seemingly unsystematic distribution of the data points, we can identify qualitative differences which can be used to interpret the results. For example, both shingle layouts show nonzero power outputs up to a fully shaded PV solar module ($A_{\mathrm{sh}} = 1$). In contrast to that there is no power output to be expected from the butterfly module for $A_{\mathrm{sh}} > 0.8$. In case of the conventional layout this is even more severe, and the power output rapidly drops to zero for $A_{\mathrm{sh}} > 0.2$. There are few exceptions from this and most prominent are the data points which involve one or multiple conductive bypass diodes in the simulated scenario. These states can be identified by a distinct horizontal accumulation of data points, as indicated by the black arrows.

In case of both shingle and the conventional layout there are two whereas the butterfly layout displays five such diode levels.

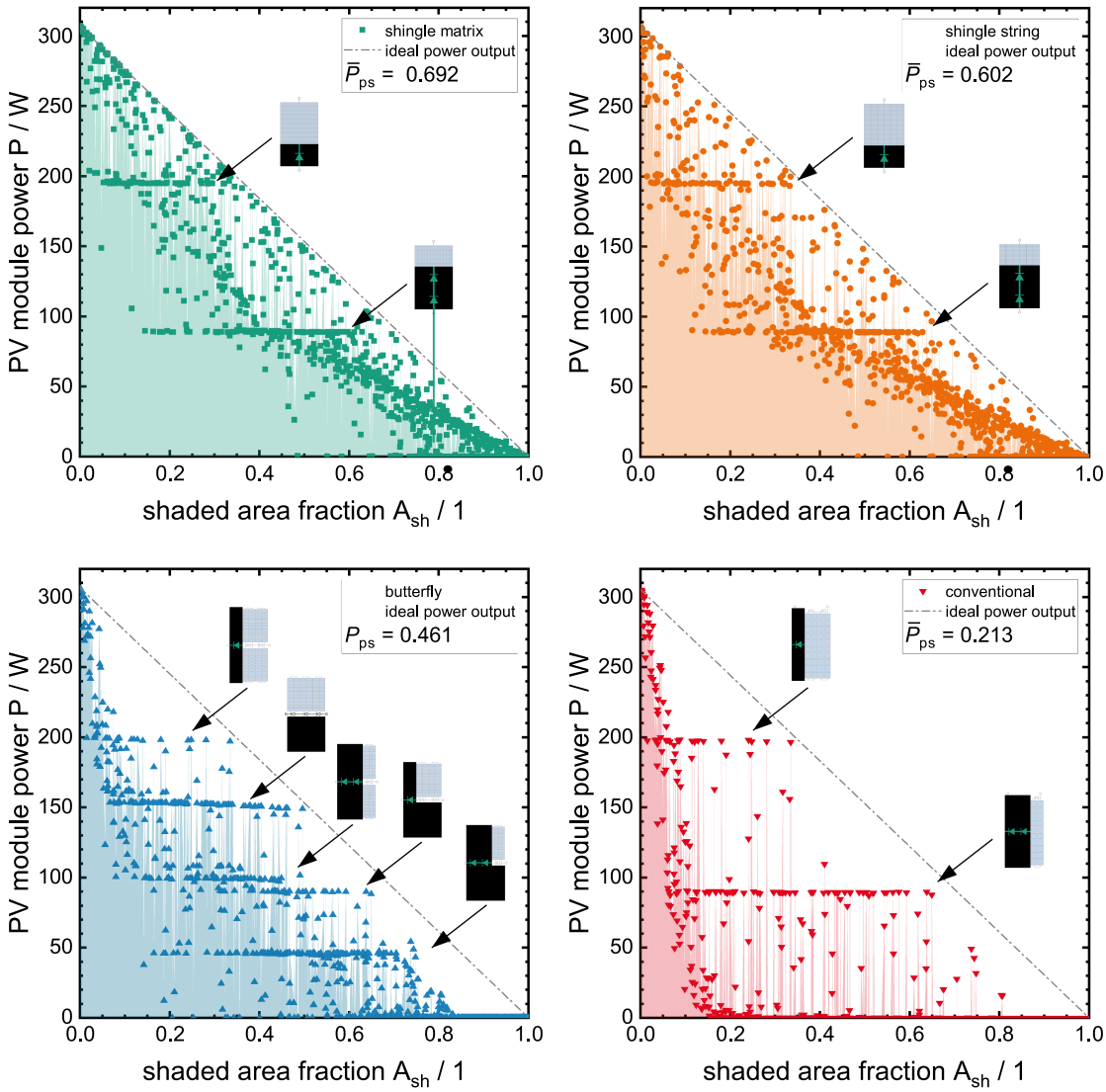

Fig. 7. Results of the LHS study for rectangular shadows. Each graph contains the data points for one module layout with its ideal power output as dash-dotted line. The area below $\boldsymbol{P}(\boldsymbol{A}_{\mathbf{sh}})$ is highlighted and $\bar{\boldsymbol{P}}_{\mathbf{ps}}$ computed according to (7) given in the legend. Several horizontal lines corresponding to cases where at least one bypass diode is conductive are visible. Note, that the sketched cases of conductive bypass diodes labeling the lines are exemplary and include all possible permutations of the individual case.

The additional levels in the butterfly layout are caused by the separation of the PV solar module in an upper and a lower half, which are interconnected in parallel. In Fig. 7 all levels are identified with an exemplary schematic of the bypass diode configuration corresponding to the power level.

The evaluation of (8) yields average values of $\bar{P}_{\mathrm{ps}} = 0.692$ for the shingle matrix, $\bar{P}_{\mathrm{ps}} = 0.602$ for the shingle string (87% of the shingle matrix), $\bar{P}_{\mathrm{ps}} = 0.461$ for the butterfly (67%) and $\bar{P}_{\mathrm{ps}} = 0.213$ for the conventional interconnection (31%). One reason for the significant differences found for the $\bar{P}_{\mathrm{ps}}$ values lies in the combination of serial and parallel interconnection of the solar cells in the shingle modules. For both layouts we find many data points close to the line of the ideal power output. 11.94% and 5.23% of the data lie within 10% below the ideal power output for the shingle matrix and the shingle string layout, respectively. For the conventional and the butterfly layout only 1.64% and 1.88% respectively are found within 10% of the ideal power output. Most of these data points are close to $A_{\mathrm{sh}} = 0$, whereas in the shingle layouts the points close to ideal power output scatter over the complete range of A_{sh}. When shading strikes under large angles α_{sh} close to 90 °, it affects shingle PV solar modules perpendicular to the parallel interconnection. In these cases, shingle PV solar modules suffer only losses proportional to the width of the shading covering the module. We can therefore state that shingle PV solar modules respond ideally to such shading scenarios, which is not achievable by the other layouts to this degree.

Other than the shingle string, the shingle matrix interconnection allows lateral current flows as discussed in previous work [13]. This becomes most relevant for a wide angular width around the module diagonal. Resulting from this, even more data points are close to the ideal response and a difference of $\Delta\, \bar{P}_{ps} = 9\%_{\mathrm{abs}}$ higher compared to the shingle string interconnection is found.

Overall, the distinct differences between the investigated module layouts indicate, that the interconnection scheme can

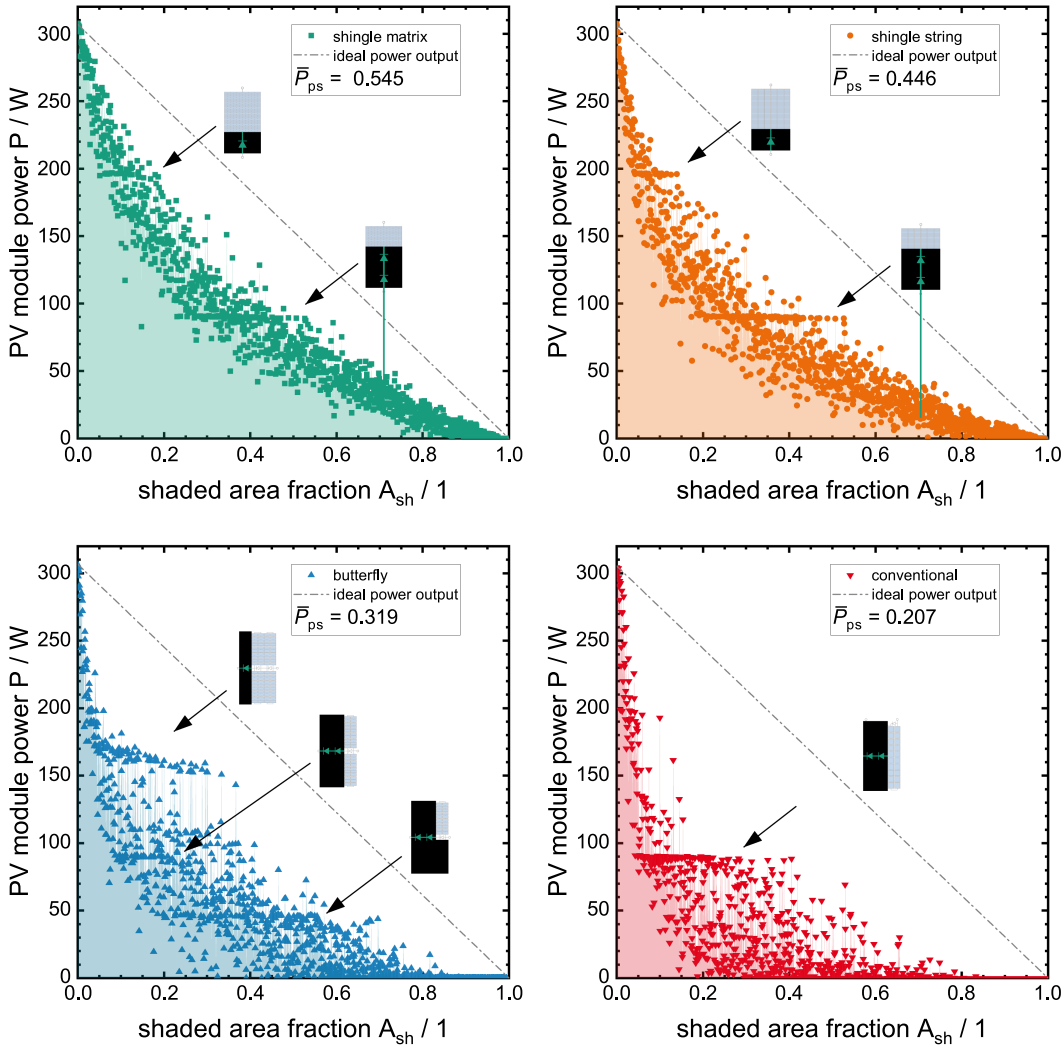

Fig. 8. Results for random shading of PV modules. Each graph contains the data points for one module layout with its ideal power output as dash-dotted line. The area below $\boldsymbol{P}(\boldsymbol{A_{sh}})$ is highlighted and $\bar{\boldsymbol{P}}_{\mathbf{ps}}$ computed according to (7) given in the legend. We find less distinct horizontal lines compared to rectangular shading corresponding bypass diode in conductive states.

have a large impact on the shading response of the PV solar modules when partially shaded by rectangular objects, of up to factor 3 to 4.

C. $\bar{\boldsymbol{P}}_{\mathbf{ps}}$ *for Random Shading*

Fig. 8 shows the data obtained for random shading in the same manner as presented for rectangular shading in the last section. Again $P(A_{\mathrm{sh}})$ is derived from the power output of every individual simulated scenario. $\bar{P}_{\mathrm{ps}}$ is evaluated similar to Fig. 7 and the values given in the legend of each layer. Again, we find significant differences in $\bar{P}_{\mathrm{ps}}$ with values of $\bar{P}_{\mathrm{ps}} = 0.545$ for the shingle matrix $\bar{P}_{\mathrm{ps}} = 0.446$ for the shingle string $\bar{P}_{\mathrm{ps}} = 0.319$ for the butterfly, and $\bar{P}_{\mathrm{ps}} = 0.207$ for the conventional interconnection. The ranking between the layouts is identical to the rectangular shading scenario however with lower absolute values. We propose that the reason for this is inherent for the considered basic shading shape. In rectangular shading, there is a certain probability that only a part of the module, bypassed by a protective diode, is affected. Random shading as investigated in this article will with a high probability affect multiple parts of the module resulting in less conductive bypass diode states and hence an overall reduced power output. This assumption is supported by the fact that the data in Fig. 8 exhibit less distinct levels of conductive bypass diode states and appear more scattered especially for powers below 100 W (butterfly and conventional layout).

It seems remarkable that the shingle layouts show a more evenly decay with A_{sh} , almost like an exponential dependence of $P(A_{\mathrm{sh}})$. However, we currently do not have a physically motivated explanation for this, especially since the two other layouts do not show such a behavior and therefore besides stating the observation leave a possible explanation to future work.

Fig. 9 summarizes the results for evaluation of $\bar{\boldsymbol{P}}_{\mathbf{ps}}$ for both investigated basic shading scenarios and all four investigated PV module layouts. As we used LHS is capable to represent the multidimensional parameter space $\bar{\boldsymbol{P}}_{\mathbf{ps}}$ incorporates a high expressiveness. For example, we can conclude that e.g., for

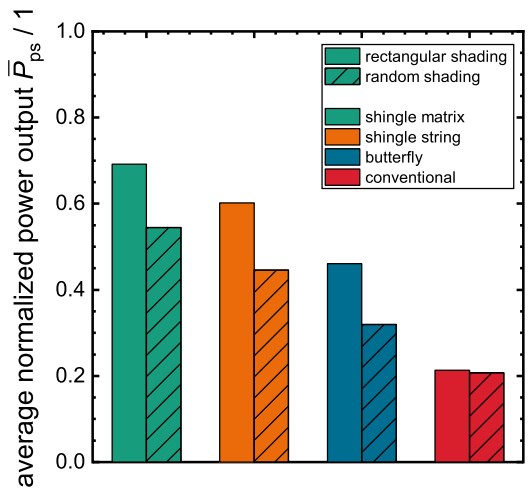

Fig. 9. Comparison of $\bar{\boldsymbol{P}}_{\mathbf{ps}}$ for all layouts and both shading cases.

locations involving rectangular shading a shingle matrix module with $\bar{\boldsymbol{P}}_{\mathbf{ps}} = 0.692$ is expected to yield approximately 3 to 4 times more energy compared to the conventional interconnection with $\bar{\boldsymbol{P}}_{\mathbf{ps}} = 0.213$ (without taking into account the potentially higher nominal capacity of a shingle module). In the same manner, a shingle matrix module is expected to yield approximately 70% of the energy an ideal interconnection of solar cells which does not suffer from overproportionate shading losses would yield.

As such information becomes more useful for the growing use cases of integrated PV, e.g., BIPV and VIPV we see a growing need to include such ratings in solar module data sheets in the near future.

V. Conclusion

In this article, we discussed an important approach already taken and now proposed by our group to access the shading resilience of solar modules. The key features of our approach involve the definition of basic shading shapes and the demand to distribute random shading scenarios equidistantly with respect to their shaded area fraction A_{sh}. We conduct large-scale Monte Carlo simulations, partly governed by LHS with more than 3000 investigated scenarios in total.

Our results show differences in $\bar{P}_{\mathrm{ps}}$ for four module layouts compared in both rectangular and random shading. However, in both cases the shingle solar modules show significant advantages over the butterfly and conventional interconnections. We find, that in general rectangular shading leads to higher values of $\bar{P}_{\mathrm{ps}}$ since bypass diodes reduce losses more often and effective than in case of randomly distributed shaded areas. The results in general show that from the currently existing solar module layouts shingle solar cell modules offer the highest potential to increase the energy yield in environments where shading is frequently affecting the solar modules.

Although we presented validation experiments of rectangular shading scenarios in a previous publication [13], future work could focus on further experimental validation. Field testing of solar modules subjected to dynamic shadings could indicate the impact on energy yield for the different layouts.

Although some approaches already exist, values to quantify the response of solar modules still rely on experimental or numerical investigation of many different scenarios. We show, that by our approach 200–400 scenarios per basic shading case already produce robust average values. This can be used as a baseline for further improvement including the formulation of further basic shading shapes and a weighting function or vector for different sites and applications (vehicle or building integration, roof top or power plant installations). We see the need of such information in PV module data sheets in the future to account for the growing diversity in PV applications, which also has already been demanded in other work [2], [40].

Acknowledgment

The author thanks all his co-authors for their contributions and fruitful discussions. A special thanks to H. Riesch-Oppermann of the IAM-WBM at KIT for fruitful discussions on stochastics. We also want to thank Dr. rer. nat Jonas Huyeng from Fraunhofer ISE for his critical review and helpful remarks to our work. We thank the German Federal Environmental Foundation for supporting our work with a Ph.D. scholarship grant.

References

[1] U. Jahn and W. Nasse, "Operational performance of grid-connected PV systems on buildings in Germany," *Prog. Photovolt.*, vol. 12, no. 6, pp. 441–448, 2004.

[2] H. Ziar *et al.*, "Quantification of shading tolerability for photovoltaic modules," *IEEE J. Photovolt.*, vol. 7, no. 5, pp. 1390–1399, Sep. 2017, doi: 10.1109/JPHOTOV.2017.2711429.

[3] R. Eke and C. Demircan, "Shading effect on the energy rating of two identical PV systems on a building façade," *Sol. Energy*, vol. 122, pp. 48–57, 2015.

[4] C. Schuss, T. Kotikumpu, B. Eichberger, and T. Rahkonen, "Impact of dynamic environmental conditions on the output behaviour of photovoltaics," in *Proc. 20th Int. Symp. 18th Int. Workshop ADC Model. Testing Res. Elect. Electron. Meas. Econ. Upturn*, 2014, pp. 993–998.

[5] Deutsche Gesellschaft für Sonnenenergie, *Planning and Installing Photovoltaic Systems: A Guide For Installers, Architects and Engineers*, 3rd ed. London, U.K.: Routledge, 2013. [Online]. Available: http://site.ebrary.com/lib/hawhamburg/docDetail.action?docID=10737858

[6] D. Götz *et al.*, "Evaluation of shading tolerance of PV modules with different module designs for mobile applications by simulation, indoor and outdoor measurements," in *Proc. 36th Eur. Photovolt. Sol. Energy Conf. Exhib.*, 2019, pp. 1–6.

[7] K. Brecl, M. Bokalič, and M. Topič, "Annual energy losses due to partial shading in PV modules with cut wafer-based si solar cells," *Renewable Energy*, vol. 168, pp. 195–203, 2021.

[8] G. Beaucarne, "Materials challenge for shingled cells interconnection," *Energy Procedia*, vol. 98, pp. 115–124, 2016.

[9] A. Mondon, N. Klasen, M. Mittag, M. Heinrich, and H. Wirth, "Comparison of layouts for shingled bifacial PV modules in terms of power output, Cell-to-Module ratio and bifaciality," in *Proc. 35th Eur. Photovolt. Sol. Energy Conf. Exhib.*, 2018, pp. 1006–1010.

[10] W. R. Baron and P. F. Virobik, "Solar array shading and a method of reducing the associated power loss," in *Proc. 4th Photovolt. Specialists Conf.*, 1964.

[11] R. G. Vieira, F. M. U. de Araújo, M. Dhimish, and M. I. S. Guerra, "A comprehensive review on bypass diode application on photovoltaic modules," *Energies*, vol. 13, no. 10, 2020, Art. no. 2472.

[12] N. D. Kaushika and N. K. Gautam, "Energy yield simulations of interconnected solar pv arrays," *IEEE Trans. Energy Convers.*, vol. 18, no. 1, pp. 127–134, 2003.

[13] N. Klasen, D. Weißer, T. Geipel, D. H. Neuhaus, and A. Kraft, "Performance of shingled solar modules under partial shading," *Prog. Photovolt., Res. Appl.*, vol. 2021, pp. 1–14, 2021.
[14] A. Calcabrini, R. Weegink, P. Manganiello, M. Zeman, and O. Isabella, "Simulation study of the electrical yield of various PV module topologies in partially shaded urban scenarios," *Prog. Sol. Energy*, vol. 225, pp. 726–733, 2021.
[15] A. Alobaid and R. Adomaitis, "Monte Carlo simulation for optimal solar cell configuration," in *Proc. Comput. Aided Chem. Eng., 13th Int. Symp. Process Syst. Eng.*, 2018, pp. 1855–1860.
[16] "International technology roadmap for photovoltaic (ITRPV): 2020 results, April 2021," Int. Technol. Roadmap Photovolt., Frankfurt, Germany, Apr. 2021.
[17] R. K. Pachauri, I. Kansal, T. S. Babu, and H. H. Alhelou, "Power losses reduction of solar PV systems under partial shading conditions using reallocation of PV module-fixed electrical connections," *IEEE Access*, vol. 9, pp. 94789–94812, 2021, doi: 10.1109/ACCESS.2021.3093954.
[18] R. Witteck, M. Siebert, S. Blankemeyer, H. Schulte-Huxel, and M. Kontges, "Three bypass diodes architecture at the limit," *IEEE J. Photovolt.*, vol. 10, no. 6, pp. 1828–1838, Nov. 2020, doi: 10.1109/JPHOTOV.2020.3021348.
[19] C. A. Fernandes, J. P. N. Torres, P. C. Branco, J. Fernandes, and J. Gomes, "Cell string layout in solar photovoltaic collectors," *Energy Convers. Manage.*, vol. 149, pp. 997–1009, 2017.
[20] F. Lu, S. Guo, T. M. Walsh, and A. G. Aberle, "Improved PV module performance under partial shading conditions," *Energy Procedia*, vol. 33, pp. 248–255, 2013.
[21] A. Dolara, G. C. Lazaroiu, S. Leva, and G. Manzolini, "Experimental investigation of partial shading scenarios on PV (photovoltaic) modules," *Energy*, vol. 55, pp. 466–475, 2013.
[22] E. Paraskevadaki and S. Papathanassiou, "Estimation of PV array power losses due to partial shading," in *Proc. 25th Eur. Photovolt. Sol. Energy Conf. Exhib./5th World Conf. Energy Convers.*, 2010, pp. 4560–4564.
[23] N. Rakesh and T. V. Madhavaram, "Performance enhancement of partially shaded solar PV array using novel shade dispersion technique," *Front. Energy*, vol. 10, no. 2, pp. 227–239, 2016.
[24] R. Ramaprabha and B. L. Mathur, "A comprehensive review and analysis of solar photovoltaic array configurations under partial shaded conditions," *Int. J. Photoenergy*, vol. 2012, pp. 1–16, 2012.
[25] Q. Li, L. Zhu, Y. Sun, L. Lu, and Y. Yang, "Performance prediction of building integrated photovoltaics under no-shading, shading and masking conditions using a multi-physics model," *Energy*, vol. 213, 2020, Art. no. 118795.
[26] V. Quaschning and R. Hanitsch, "Influence of shading on electrical parameters of solar cells," in *Proc. 25th IEEE Photovolt. Specialists Conf.*, 1996, pp. 1287–1290.
[27] B. Meyers, M. Mikofski, and M. Anderson, "A fast parameterized model for predicting PV system performance under partial shade conditions," in *Proc. IEEE 43rd Photovolt. Specialists Conf.*, 2016, pp. 3173–3178.
[28] S. Mishra, H. Ziar, O. Isabella, and M. Zeman, "Selection map for PV module installation based on shading tolerability and temperature coefficient," *IEEE J. Photovolt.*, vol. 9, no. 3, pp. 872–880, May 2019, doi: 10.1109/JPHOTOV.2019.2900695.
[29] Y.-J. Wang and R.-L. Sheu, "Probabilistic modeling of partial shading of photovoltaic arrays," *Int. J. Photoenergy*, vol. 2015, pp. 1–10, 2015.
[30] N. Klasen, D. Weißer, T. Geipel, D. H. Neuhaus, and A. Kraft, "Performance of shingled solar modules under partial shading," *Prog. Photovolt. Res. Appl.*, vol. 2021, pp. 1–14, 2021.
[31] M. A. Sattler and S. Sharpies, "Field measurements of the transmission of solar radiation through trees," in *Advances In Solar Energy Technology*. Amsterdam, The Netherlands: Elsevier, 1988, pp. 3846–3850.
[32] H. S. Rauschenbach, *Solar Cell Array Design Handbook: The Principles and Technology of Photovoltaic Energy Conversion*. New York, NY, USA: Van Nostrand Reinhold, 1980.
[33] J. W. Bishop, "Computer simulation of the effects of electrical mismatches in photovoltaic cell interconnection circuits," *Sol. Cells*, vol. 25, no. 1, pp. 73–89, 1988.
[34] C. E. Clement, J. P. Singh, E. Birgersson, Y. Wang, and Y. S. Khoo, "Illumination dependence of reverse leakage current in silicon solar cells," *IEEE J. Photovolt.*, vol. 11, no. 5, pp. 1285–1290, Sep. 2021, doi: 10.1109/JPHOTOV.2021.3088005.
[35] A. Calcabrini, M. Muttillo, R. Weegink, P. Manganiello, M. Zeman, and O. Isabella, "A fully reconfigurable series-parallel photovoltaic module for higher energy yields in urban environments," *Renewable Energy*, vol. 179, pp. 1–11, 2021.
[36] J. C. Helton and F. J. Davis, "Latin hypercube sampling and the propagation of uncertainty in analyses of complex systems," *Rel. Eng. Syst. Safe*, vol. 81, no. 1, pp. 23–69, 2003.
[37] M. D. Mckay, R. J. Beckman, and W. J. Conover, "A comparison of three methods for selecting values of input variables in the analysis of output from a computer code," *Technometrics*, vol. 21, no. 2, pp. 239–245, 1979.
[38] H. A. Steinberg, "Generalized quota sampling," *Nucl. Sci. Eng.*, vol. 15, no. 2, pp. 142–145, 1963.
[39] D. Raj, *Sampling Theory: MCGraw-Hill Series in Probability and Statistics*. New York, NY, USA: McGraw Hill, 1968.
[40] H. Ziar, S. Mishra, O. Isabella, and M. Zeman, "The need for a new parameter on PV modules datasheet: Shading tolerability," in *Proc. IEEE 7th World Conf. Photovolt. Energy Convers.*, 2018, pp. 664–667.